

50 Years of Compounds Semiconductors at the Institute of Electron Technology, Warsaw

A. PIOTROWSKA^{a,*}, E. KAMIŃSKA^b AND M. BUGAJSKI^a

^a*Łukasiewicz Research Network, Institute of Microelectronics and Photonics, al. Lotników 32/46, 02-668 Warsaw, Poland*

^b*Institute of High Pressure Physics, Polish Academy of Sciences, al. Prymasa Tysiąclecia 98, 01-142 Warsaw, Poland*

Doi: [10.12693/APhysPolA.142.575](https://doi.org/10.12693/APhysPolA.142.575) *e-mail: anna.piotrowska@imif.lukasiewicz.gov.pl

In 2022, we are celebrating the 50th anniversary of the “Jaszowiec” International School & Conference on the Physics of Semiconductors. One of the highlights of this anniversary was the reminiscence session at the Jaszowiec 2022 meeting, recalling the most important achievements in the field of semiconductor physics and technology in the institutions organising the Conference. This paper aims to highlight the accomplishments of the Institute of Electron Technology, Warsaw, with particular emphasis on II–VI and III–V compounds and their application in electronic and optoelectronic devices. Specifically, the review covers narrow-gap HgCdTe for galvanomagnetic devices, GaAs-, GaP-, InP-, and GaSb-based materials for optoelectronics and photonics, SiC and GaN for radio-frequency and high-power electronics, and finally ZnO and InGaZnO for transparent electronics and sensors. Research results on device physics, material development, device design, and processing are presented.

topics: ohmic contacts, galvanomagnetic devices, electron devices, semiconductor lasers

1. Introduction

2022 marks the 50th anniversary of the “Jaszowiec” International School & Conference on Physics of Semiconductors.

This paper is an addendum to the presentation “50 years of Compound Semiconductors at the Institute of Electron Technology, Warsaw”, which was given during the reminiscence session of the “Jaszowiec 2022” meeting, held in June 2022. The main goal of the paper is to outline the most important accomplishments of the Institute of Electron Technology (ITE) in the area of III–V and II–VI compound semiconductors. The intention is also to commemorate the people who laid the foundation for this research and inspired next generations of researchers. Where useful, the paper also addresses the issue of research infrastructure.

Three main parts of the paper correspond to the time periods, in which there were fundamental changes in the organization of institute research. The first is the period when ITE was part of the Polish Academy of Sciences, the second is the time of activities in the Semiconductor Research and Production Centre, and the third started with obtaining a legal personality and joining the European Research Area.

2. Foundation of the Institute of Electron Technology, Polish Academy of Sciences (ITE PAN)

There are three dates that mark the beginning of ITE PAN.

- In 1952, Professor Janusz Groszkowski was appointed as the head of the newly created Department of Electronics at the Division of Technical Sciences of the Polish Academy of Sciences with the mission of conducting fundamental and applied research in the novel emerging discipline — semiconductor electronics.

Professor Groszkowski was a person of outstanding scientific achievements and merits, a highly respected man. After graduating from the Warsaw Polytechnic (now the Warsaw University of Technology), he was one of the youngest professors of this academy, and at the same time the founder and director of the Institute of Telecommunication. Groszkowski was also a renowned specialist in the field of radio engineering, the father of Polish electronics. During the Second World War, he took part in the resistance movement, and in the course of his underground activity at the Warsaw Polytechnic, he

was the one who decoded the control system of the German V2 missiles. After the Second World War, he was a professor at the Warsaw Polytechnic, Faculty of Telecommunication (later Electronics) and a member of Polish Academy of Sciences, and for several years its president [1]. Therefore, this was the first seed that led to the creation of the Institute of Electron Technology.

- In 1953, the Department became part of the Institute of Fundamental Technological Research, Polish Academy of Sciences (IPPT PAN).
- Finally, in 1966, ITE was formally established, being organized on the basis of three units: the Department of Electronics and the Department of Magnetics of the Institute of Fundamental Technological Research, Polish Academy of Sciences, and the Department of the Semiconductor Technology of Institute of Physics, Polish Academy of Sciences. The first director of ITE was Professor Bohdan Paszkowski, and the scientific deputy director — Professor Witold Rosiński. And again, two excellent scientists, Professors of the Warsaw University of Technology, Faculty of Electronics, took the lead of the Institute [2, 3].

The laboratories of the Electronics Department PAS were initially located in the Staszic Palace at Krakowskie Przedmieście, and partly in the building of the Radio Engineering at Koszykowa 57 at the campus of the Warsaw University of Technology. Then they were transferred to Świętokrzyska 21, to the Bank's building, until the completion of the final premises at al. Lotników 32/46.

Working conditions in the Institute at that time were truly Spartan, with technological equipment built independently, and parts obtained wherever possible [4]. Many electronic measuring instruments were constructed according to the researchers' own designs. But the staff was enthusiastic, composed mostly of young graduates from the Faculty of Communication (later Electronics) of the Warsaw University of Technology, former students of Professor Groszkowski. It should be emphasized that the Professor was not only outstanding scientist and respected lecturer, but also a very warm person widely admired by students and staff.

In the ITE PAN's laboratories, the first Polish germanium and silicon diodes and transistors were developed, together with the first optoelectronic devices — gallium arsenide infrared radiation sources shown in Fig. 1 [5, 6], and silicon photodetectors. Also, world's most original technologies of manganese-cobalt and manganese-cobalt-aluminium thermistors and mercury cadmium telluride (HgCdTe) Hall generators were elaborated there.

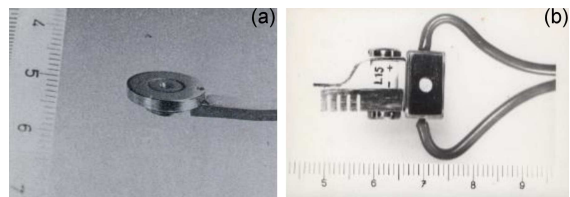


Fig. 1. First optoelectronic devices fabricated at ITE PAN [5–6]: (a) GaAs LED 3 (1964), (b) GaAs laser diode (1965).

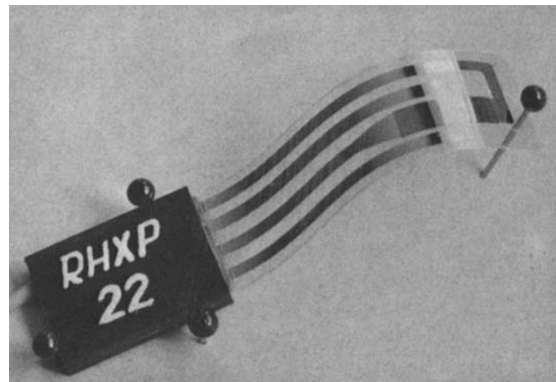


Fig. 2. Hall probe RHXP22 ($\text{Cd}_{0.09}\text{Hg}_{0.91}\text{Te}$) [10].

At this point, it is worth mentioning that the alloy system HgTe–CdTe was then a hot topic of semiconductor physics and the subject of very intensive fundamental and applied research. In particular, it was the focus in a number of early national seminars on the $\text{A}^{\text{II}}\text{B}^{\text{VI}}$ group semiconductors in Jaszowiec.

HgCdTe is characterised by a continuous transition from negative to positive energy gap with varying CdTe content, enabling the operation of semiconductor detectors in the range 1–15 μm . Other features are extremely small effective masses (of the order of $0.0004 m_0$) and, related to them, very high mobilities (over $10^6 \text{ cm}^2/(\text{V s})$ at 4.2 K) for compositions close to 9 at% CdTe. All this made it possible to construct galvanomagnetic devices and this was the direction that Doctor Stanisław A. Ignatowicz and his team at ITE have chosen. The originality of their approach relied on the use of $\text{Cd}_x\text{Hg}_{1-x}\text{Te}$ in the form of a thin film and the choice of mica as the substrate material. The result of extensive work, involving the study of electrical properties and microstructure, was the development of an original technology of the thin CdHgTe films fabrication by using vacuum deposition techniques and thermal treatment in a mercury vapour and argon atmosphere [7–9]. They were successfully applied in various model devices, i.e., basic model shown in Fig. 2, double Hall-probe, ferrite Hall-probe, and helium Hall-probe [10–12]. It should be stressed that all these devices, as well as other developed in the Institute, were produced on laboratory scale at the Experimental Manufacturing Unit of ITE PAN.

3. Institute of Electron Technology in the Semiconductor Research and Production Centre

3.1. III–V semiconductors for optoelectronics

From the very beginning, the hallmark of ITE was optoelectronics based on III–V semiconductors. The research behind it was initiated and guided, for more than twenty years, by Professor Bohdan Mroziewicz, one of the most brilliant and distinguished ITE scientists, professionally active until the last years of his life.

The onset of the optoelectronic research can be formally associated with the fabrication of the first GaAs light-emitting diodes (LEDs) in 1964, followed by the first GaAs laser diode in 1965. In the 1970s, research covered the entire spectrum of compound semiconductors based on GaAs, GaP, and InP.

An important factor defining the character of these research was the transfer in 1970 of ITE from the Polish Academy of Sciences to the newly created Semiconductor Research and Production Centre (NPCP), where ITE was to provide novel solutions for the TEWA semiconductor factory. To cope with this task, the research laboratories have been organised in such a manner as to ensure a complete value chain, from device design to final measurements and reliability tests.

The basic technologies for the fabrication of III–V optoelectronic structures were liquid-phase epitaxy and diffusion. Single and double heterostructures AlGaAs/GaAs on GaAs substrate, GaP and InGaP on GaP substrate, and InGaAsP on InP substrate were developed. Several material-dedicated LPE reactors were built for this goal. At the same time, an effort had been undertaken to create a clean room with a complete technological line for processing of the III–V device structures. It was the first and for decades the only technological laboratory of this type in Poland, constantly modernized, cooperating with many research institutions, and providing research services. Without risk one can say that most of the III–V and II–VI semiconductor samples in Warsaw received ohmic contacts there.

The research and development (R&D) works implemented in the industry included a whole range of different types of III–V optoelectronic devices, the most important of which are GaAs infrared LEDs, AlGaAs ($\lambda = 670$ nm), GaP ($\lambda = 690$ nm), GaAsP ($\lambda = 660$ nm) red LEDs, GaInP ($\lambda = 565$ nm) green LEDs, GaAsP semiconductor displays, fiber optic diodes based on the double heterostructure AlGaAs/GaAs ($\lambda = 0.8\text{--}0.9$ μm), GaInAsP/InP ($\lambda = 1.3$ μm), PIN photodiode GaInAsP/InP ($\lambda = 1.3$ μm), and finally double heterostructures AlGaAs/GaAs high-power infrared lasers, and double heterostructure GaInAsP/InP lasers for the 1.3 μm band. A few examples of LEDs and LDs in serial production are displayed in Fig. 3.

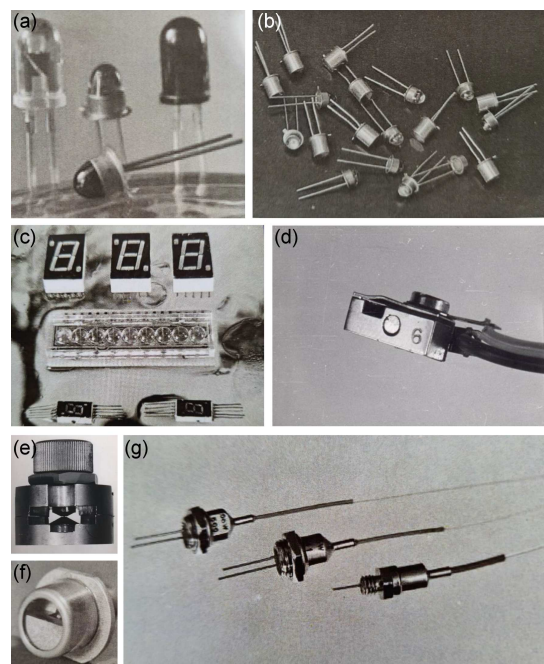


Fig. 3. (a) Infrared GaAs LEDs (1967) [14], (b) red (AlGaAs) and green (GaInP) LEDs (1974) [14], (c) red GaAsP display (1975) [14], (d) GaAs LD (1966), (e) GaAs LD (1967) [14], (f) DH AlGaAs/GaAs IR high-power LD (1984) [14], (g) DH AlGaAs/GaAs fiber optic LEDs (1986) [14].

A more detailed description of R&D activity in the field of III–V optoelectronics can be found in the review paper [13], which is part of the special volume of “Elektronika”, celebrating 20 years of ITE PAN/CEMI (CEMI — Naukowo-Produkcyjne Centrum Półprzewodników). The overall picture, seen from the perspective of half a century, is described in the golden jubilee paper [14].

The above success resulted from the joint effort of many people at the Institute. The close cooperation of various teams was absolutely necessary. Technology of advanced semiconductor devices required not only progress in terms of epitaxial growth, but also in every individual processing step. One of them was the ohmic metal/semiconductor contacts technology.

3.2. Metallization and processing of III–V semiconductor structures

The term “ohmic” refers in principle to a contact that is noninjecting and has a linear I – V characteristics in both directions. In practice, a contact is considered ohmic if the voltage drop across it is much smaller than that across the device. The linearity of the I – V relationship is less important, provided that the contact resistance is very small compared with the device resistance. The most relevant parameter describing the electrical performance of the ohmic metal/semiconductor (m/s) contact is its resistivity given by $\rho_c = [(dJ/dV)|_{V=0}]^{-1}$. Other

important features of ohmic contacts in semiconductor devices are their structural homogeneity, fine pattern capability, smoothness of surface and m/s interface, limited in-depth penetration, limited stresses, high electrical and thermal conductivity, high corrosion resistance, and high reliability.

The vast majority of m/III–V combinations form depletion layer contacts (usually rectifying or blocking), and the conduction properties of such contacts are dominated by the actual transport mechanism, which can be due to (i) thermionic emission (TE) of carriers over the top of a barrier (which give rise to current rectification), (ii) thermionic-field emission (TFE), i.e., tunnelling of hot carriers through the top of the barrier (when high doping levels of semiconductor narrow the depletion layer), and (iii) field emission (FE), i.e., carrier tunnelling through the entire barrier, which is the preferred mode of current transport in ohmic contacts. In this case, r_c is determined predominantly by the factor $\exp(\Phi_B/E_{oo})$, where Φ_B is the barrier high and

$$E_{oo} = \frac{qh}{2\sqrt{N_{D,A}/(m^* \varepsilon)}} \quad (1)$$

is the tunnelling parameter. Here, $N_{D,A}$ is the dopant concentration, m^* is the effective mass of tunnelling carriers in the semiconductor, ε its permittivity, q is electronic charge, h is Planck's constant. In fact, E_{oo} is a very useful parameter in predicting the blocking or ohmic characteristics of a metal–semiconductor contact. For $k_B T/E_{oo} \gg 1$, the thermionic process dominates and the contact behaves as a Schottky barrier. For $k_B T \ll 1$, the field emission dominates and the contacts exhibit ohmic characteristics.

Therefore, there are basically two possible ways to achieve ohmic contact. One consists of having or creating a highly doped subcontact region adjacent to the metal. In such a case, the barrier width is so thin that field emission dominates and the contact is ohmic. The second approach consists of having a low potential barrier at the metal–semiconductor interface. The properties of the contact depend considerably of the choice of metallic layers (including dopant, which should be introduced into the subcontact film during thermal processing), their thickness, composition and method of deposition, surface preparation, and heat treatment procedure. An overview of fabrication techniques of ohmic contacts to III–V semiconductors can be found in references [15–18].

In practice, gold-based metallizations deposited by vacuum techniques and subjected to heat treatment were commonly used. They presented a number of advantages, in particular sufficiently low contact resistance, but also had a number of serious drawbacks, the most important of which was the nonhomogeneity of the metal/semiconductor interface and deep protrusions penetrating the semiconductor subcontact region, which translated into limited reliability.

Consequently, comprehensive research was undertaken at ITE to better understand and control the processes of ohmic contact formation. The focus was on contacts to GaAs [19–36], comparative studies involved contacts to InP, GaP, and GaSb [20, 37–42]. Metallizations were deposited by vacuum evaporation, and post-deposition heat treatments were performed in the flow of H_2 or H_2/N_2 . Several complementary techniques, namely XRD (X-ray diffraction), EDX (energy-dispersive X-ray spectroscopy), RBS (Rutherford backscattering spectrometry), SIMS (secondary ion mass spectrometry), SEM (scanning electron microscopy), and XTEM (cross-sectional transmission electron microscopy), were used to characterise the evolution of contact microstructure at various stages of contact formation.

An important aspect of the applied research methodology was the analysis of the escape of volatile group V elements from the contact area, for which the technique of their quantitative measurements — the so-called Cr-collector method — was developed [22]. The method relies on the use of a thin Cr film to capture volatile species, and their subsequent analysis is performed with the RBS technique. Cr-collectors were prepared by sputter deposition of 100 nm thick Cr film onto Si/SiO₂ substrates. During thermal processing, they were placed face-to-face on top of the metallized semiconductor surfaces.

Much of the knowledge about the mechanism of formation Au-based ohmic contacts was derived from the thermal reaction of pure Au with elements from the groups III–V. The marked ability of the group III element in the semiconductor substrate to react with gold appeared to be a common feature of the investigated systems. No reaction product involving the group-V element was observed in contacts on GaAs and GaP, whereas the Au₂P₃ phase was identified in contacts on InP [37, 38] and the AuSb₂ phase in contacts on GaSb [41, 42].

Ternary phase diagrams were helpful in interpreting these data, if used carefully, as they refer to closed systems, while conventional contact annealing is performed in open systems where evaporation of group V elements is possible. The most noticeable effect of closing the contact system during heat treatment was observed for Au/GaAs contacts [19, 20, 40]. In an open system, gallium reacted with GaAs to form double phases (α -AuGa, Au₇Ga₂), Au₂Ga, AuGa), while arsenic evaporated through the metal layer at a higher rate than for the free GaAs surface. The alloyed metallization appeared highly nonuniform both laterally and vertically with respect to the initial semiconductor surface. A typical picture of the resultant interface consisted of metallic inclusions, rectangular on the (100) surface, triangular on (111), penetrating GaAs to a depth of the order of the thickness of the Au layer. In a closed system,

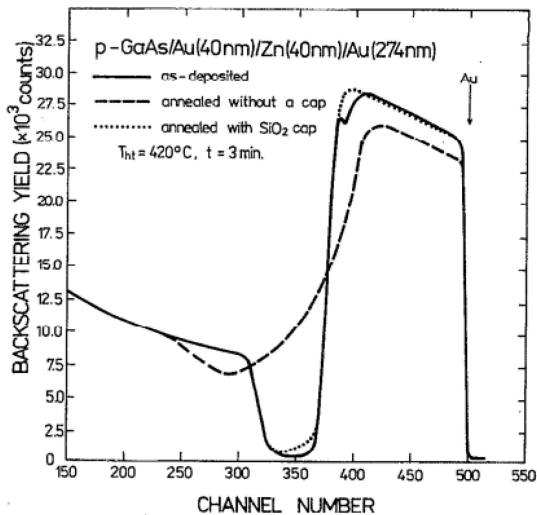


Fig. 4. The RBS (2 MeV He^+) spectra of as-deposited and heat treated (at 420°C for 3 min) standard metallization 40 nm Au/40 nm Zn/274 nm Au/p-GaAs annealed either with SiO_2 cap or without it [22].

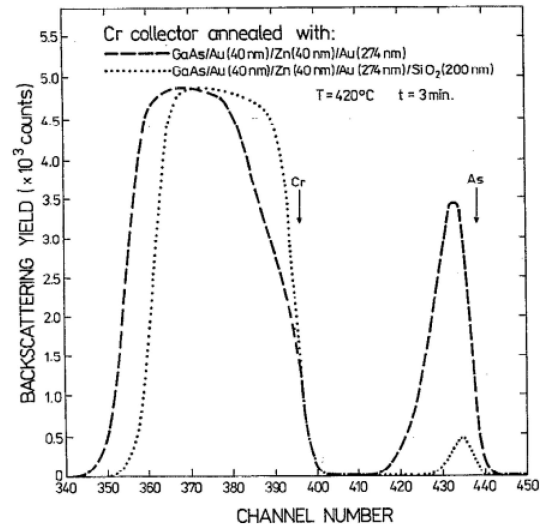


Fig. 5. The RBS (2 MeV He^+) spectra of Cr collectors annealed in contact with unprotected and SiO_2 -capped 40 nm Au/40 nm Zn/274 nm Au metallization on GaAs [22].

owing to the suppressed vaporization of As, the reaction between Au and GaAs was restrained, and the α -AuGa phase was stable in contact with GaAs.

The introduction of dopants into Au metallization caused important changes in the kinetics of the contact reaction and the phase composition of the contact region. In order to clarify these issues, a series of experiments comparing the annealing behaviour of Au(Zn)/p-GaAs, Au(Ge)/n-GaAs, and Au(Te)/n-GaAs were performed [21–28]. Zn, Te, and Ge were chosen as dopants, which are electrically active when placed in the GaAs lattice on specific sites. Thus, Zn occupies Ga sites, Te requires As vacancies to be active, Ge is an amphoteric dopant. In order to precisely control the initial composition of the metallization, it was deposited in the form of a layered structure. The contacts were annealed in two configurations — either with or without an encapsulating SiO_2 layer. It was expected that in a closed system, the thermally activated reaction between Au and GaAs preferentially creates the Ga vacancies required for Zn and Ge atoms to form acceptors and donors, respectively. As for arsenic, which is insoluble in Au, it could accumulate at the metal/GaAs interface and/or create antisite As_{Ga} defects. Thus, annealing under the capping layer may reduce the availability of the As vacancies in the interfacial region, and the Te atoms would serve as a probe for the availability of such sites.

The most meaningful result of these experiments was the dissimilarity of Au(Te)/n-GaAs contacts annealed in a closed system. While both the Au(Zn)/p-GaAs and Au(Ge)/n-GaAs

contacts exhibited excellent ohmic properties when annealed with an insulating cap, the Au(Te)/n-GaAs contacts exhibited rectifying behaviour over the entire range of processing temperatures and times. The annealing behaviour of the capless Au(Zn)/p-GaAs, Au(Ge)/n-GaAs and Au(Te)/n-GaAs contacts was similar, i.e., it was characterised by a minimum of the specific contact resistance as a function of the annealing temperature.

The development and final microstructure of the contact region was strongly dependent on a particular dopant (its reactivity with Au and GaAs) and annealing conditions (use of the capping layer). In the following, we summarize the results for Au(Zn)/p-GaAs contacts [21–24, 27–29].

Figure 4 displays RBS spectra of as-deposited and annealed 40 nm Au/40 nm Zn/274 nm Au/p-GaAs metallization, heat treated at 420°C for 3 min either with protecting SiO_2 cap (Tkc) or unprotected (Tk), while in Fig. 5, RBS spectra of the corresponding Cr-collectors annealed together are shown. The heat treatment parameters have been optimized to obtain the minimum of the specific contact resistance. It was found that the application of Si/ SiO_2 /Cr probing samples did not alter the rate of the Au(Zn)–GaAs reaction.

The following characteristic features should be pointed out. First, the low-energy step in the Au spectrum of the as-deposited sample ensues from the low-temperature interaction of Zn and Au and the consequent formation of the AuZn (50 at.%) phase at the metal/semiconductor interface. Second, the decrease in the height of the Au spectrum of the annealed contact results from the interaction of Au with GaAs. Computer simulations

TABLE I

Outcome of contact reaction for standard metallization of 40 nm Au/40 nm Zn/274 nm Au/p-GaAs annealed either with protecting SiO₂ cap (Tkc) or unprotected (Tk)

Contact material	Heat treatment		Phase composition	Ga content in Au		As loss N _{As} [atom/cm ²]
	T [°C]	t [min]		[at%]	N _{Ga} [atom/cm ²]	
Tk	420	3	Au ₃ Zn α-Au ₃ Zn	11	1.2 × 10 ¹⁷	1.1 × 10 ¹⁷
Tkc	420	3	Au ₃ Zn α-Au ₃ Zn	0.7	7.4 × 10 ¹⁵	7.2 × 10 ¹⁵

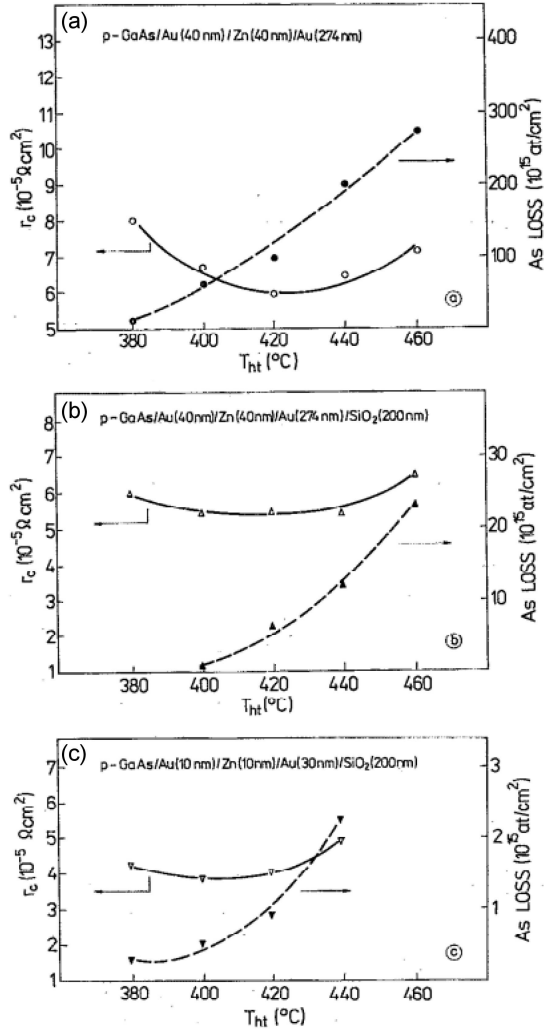


Fig. 6. Relationship between As loss, specific resistance and temperature of heat treatment for unprotected and SiO₂-capped Au(Zn) contacts to GaAs. Standard metallization of the thickness 40 nm Au/40 nm Zn/274 nm Au and thin metallization 10 nm Au/10 nm Zn/30 nm Au were used [22].

of RBS spectra using the RUMP code indicated that metallization annealed without a SiO₂ cap contains about 11 at.% of Ga atoms, while in a cap-annealed metallization, the amount of Ga atoms was about 0.7 at.%.

The arsenic signal in the RBS spectra from Cr collectors is well separated from the Cr signal. This allows for precise determination of the amount of As in the Cr matrix of the collector. The number of As atoms trapped in the Cr layer was determined by comparing the integrated yield in the As peak with the height of the Cr peak, i.e.,

$$N_{As} = \frac{A_{As}}{H_{Cr}} \frac{\sigma_{Cr}}{\sigma_{As}} \frac{E}{[\epsilon]_{Cr}^{Cr}} \quad (2)$$

Here, N_{As} is the total amount of arsenic atoms (given in atom/cm²), A_{As} is the integrated yield in the As peak, H_{Cr} is the height of the Cr peak, σ_{Cr} and σ_{As} are the Cr and As scattering cross-sections, respectively, E is the energy interval corresponding to one channel, and $[\epsilon]_{Cr}^{Cr}$ is the stopping cross-section factor for Cr. The sensitivity of As detection was estimated to be about 0.2×10^{15} atom/cm² and the efficiency of collecting As atoms to be about 90%.

The total amount of arsenic losses and the corresponding specific contact resistances are shown in Fig. 6. In Table I, the outcome of the contact reaction for standard metallization is summarized.

These data confirm that the thermally induced decomposition of GaAs strongly depends on both the presence of the capping layer and the thickness of the metallization. By using 200 nm thick insulating caps, the loss of As can be reduced by a factor of 20. Decreasing the thickness of Au(Zn) enables a further reduction in the GaAs decomposition. In particular, the formation of the thin ohmic contact 10 nm Au/10 nm Zn/30 nm Au was accompanied by a loss of As of only 6×10^{14} atom/cm², which corresponds to the release of one monoatomic GaAs layer (6.25×10^{14} atom/cm²). This suggests that the ohmic character is determined by the suitable arrangement of the bonds involving the dopant atoms at the very intimate metal-semiconductor interface, but without creating a finite layer of appreciable thickness.

In Figs. 7 and 8, plan view TEM (transmission electron microscopy) images and corresponding diffraction patterns of 80 nm Au and 20 nm Au/10 nm Zn/60 nm Au metallizations, respectively, were juxtaposed in as-deposited, capless, and cap-annealed states [29]. The results show that a very limited number of metallic intrusions have

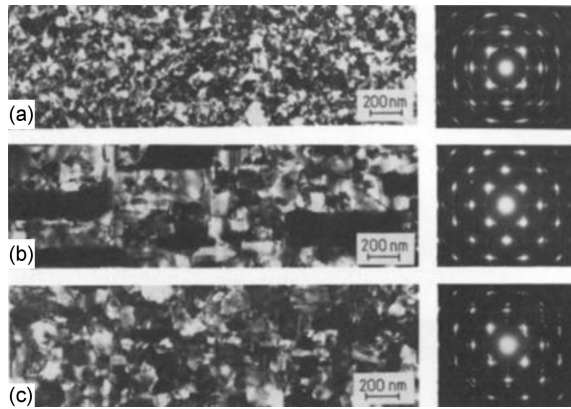


Fig. 7. Plan view TEM of 80 nm Au films: (a) unprocessed, (b) capless annealing at 420°C for 3 min, (c) annealing with a cap in the same conditions [39].

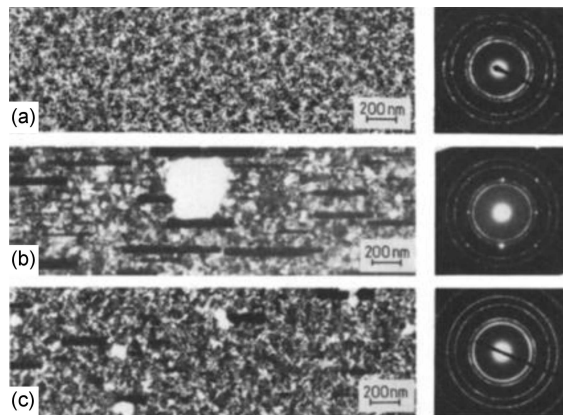


Fig. 8. Plan view TEM of 20 nm Au/10 nm Zn/60 nm Au films: (a) unprocessed, (b) capless annealing at 420°C for 3 min, (c) annealing with a cap in the same conditions [39].

formed in the capped contacts. While in the capless annealed Au/GaAs contacts, the intrusions contained about 8 at.% Ga, in the cap-annealed contacts there was less than 1 at.% Ga. The amount of Ga in the capless annealed Au(Zn) contacts was about 3.4 at.%, while in the cap-annealed contacts it was smaller than 0.2 at.%. XTEM and HREM (high-resolution transmission electron microscopy) analyses revealed the formation of R1 Au₃Zn phase at the metal/semiconductor interface of the annealed contact (Fig. 9).

These results can be interpreted in terms of a thin-film reaction between Au and GaAs. Gold itself does not react directly with GaAs but is a catalyst that decreases the activation energy of arsenic evaporation. In open systems, entropy changes driven by vapour production are the dominant driving forces for the thermal reaction between gold and GaAs. This causes the extended decomposition of GaAs and the formation of the α -AuGa phase with a high Ga content. Fast removal of excess gallium

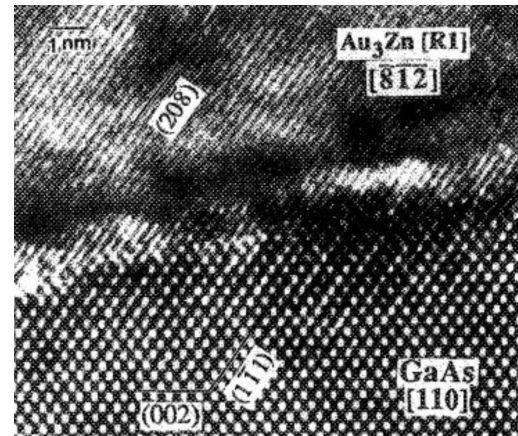


Fig. 9. HREM of the interface between the crystal grain of the R1 Au₃Zn phase and the GaAs substrate [23].

appears to be a necessary condition for arsenic to evaporate and, conversely, excessive accumulation of gallium as a factor terminating the evaporation of arsenic as well as whole reaction. By sealing the contact structure with a protective cap, the overpressure of arsenic exerted on the GaAs surface prevents excessive decomposition of the semiconductor.

As for the Au(Te)/n-GaAs contacts, no reaction between tellurium and gold was observed over the whole range of annealing temperatures. Moreover, due to its high volatility, Te sublimated in large quantities from contact annealed in an open system. In a closed system, suppression of Te sublimation activated the Te-GaAs reaction, while suppression of As vaporization restrained the Au-GaAs reaction. Ga₂Te₃ and As₂Te₃, grown epitaxially on GaAs, were the main products of the interaction, apart from unreacted Au and small quantities of Au₇Ga₂. In spite of that both Ga₂Te₃ and As₂Te₃ are low-bandgap semiconductors, their formation did not lead to the formation of ohmic contacts to n-GaAs. Annealing in the open system resulted in a heavily deteriorated interface, while the metallic film consisted of a mixture of Au and Au₇Ga₂ phase.

The metallurgy of the Au(Ge)/n-GaAs contacts presented another picture. There was no influence of the annealing configuration on the contact microstructure. The most pronounced feature of the contacts after heat treatment was the appearance of isolated Ge islands embedded in the ternary AuGeAs phase at the metal/semiconductor interface. These upper parts of the metallic layer consisted of Au and Au(Ga) phase. The only difference was that the cap-annealed contacts exhibited a smooth surface, while the surface of the unprotected contacts was rough.

The obtained results indicated that the use of Au as the main metallization component inevitably implies the choice of such dopants, which are

electrically active when placed on the Ga sites. They also indicated that Au-based ohmic contacts are more controllable than commonly believed. The beneficial role of using encapsulating cap during contact annealing has been proven.

The next step towards advanced metallization systems was to replace the insulating cap, which had to be removed after the ohmic contact formation, with conductive capping layers. The metallic cap should play a dual role — to be an encapsulant that suppresses the sublimation of volatile components of the III–V semiconductor under heat treatment and also to be a diffusion barrier preventing gold in-diffusion from the Au overlayer used for bonding and interconnection purposes [36]. Among the possible candidates for a barrier material, refractory metal nitrides and borides seemed particularly attractive because they offered an exceptional combination of properties such as high melting points, high electrical and thermal conductivity, resistance to corrosion as well as the opportunity to control their microstructure, including the most favourable — the amorphous ones. The results of comprehensive research on ZrN, ZrB₂, W₂B, and a-W₅₅B₄₅ barriers in gold-based ohmic contacts to GaAs, InP, GaP, and GaSb clearly indicated the superiority of the amorphous microstructures and directed attention to the Ti–Si–N, Ta–Si–N, and W–Ta–N systems [31–36].

The results obtained as a whole were of crucial importance not only for understanding of the process of ohmic formation, but also for practical reasons. The most important technological guideline resulting from the above research was the rationale for introducing a cap-annealing into the ohmic contacts technology, allowing for a significant reduction in the thickness of the contact metallization, limited decomposition of the semiconductor in the sub-contact region, and an effective improvement of contact homogeneity. All this was achieved with the simultaneous widening of the process window. At the same time, the merits of diffusion barriers justified their use in the metallization schemes for advanced III–V devices.

It is worth mentioning that the SiO₂ capping was successfully used to inhibit Mn interdiffusion in the CdTe/CdMnTe quantum well structures [43], while bilayer RuSi/RuSiN metallization was successfully used as an ohmic contact with increased resistance to high temperatures for thermoelectric PbMnTe-based materials [44].

4. Towards low-dimensional semiconductor structures

For the global III–V optoelectronic industry at the turn of the 1970s and 1980s it was clear that almost all the possibilities of classic heterostructures with p–n junctions had been exhausted, and new opportunities are being provided by constructions based on the use of low dimensional structures.

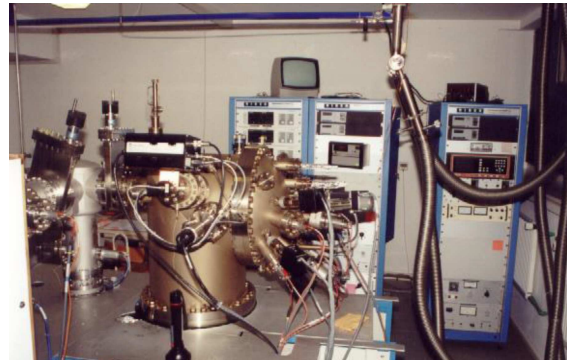


Fig. 10. The MBE Laboratory founded at ITE, headed by Professor Maciej Bugajski.

Consequently, there has been tremendous advancement in technology of semiconductor epitaxial growth around the world. Together with advanced lithographic techniques, it has become possible to produce sub-micrometre stripe structures or patterns with nanometre geometry, such as quantum wires and dots. Soon, the commercialization of reactors for molecular beam epitaxy (MBE) and metal-organic vapor phase epitaxy (MOVPE) took place as well as of equipment for electron beam (e-beam) lithography.

It became clear that without access to this type of technology in Poland, it would not be possible to stay at the forefront of semiconductor research. Therefore, an enormous attempt has been made by the entire scientific community to ensure that the awareness of this situation reached the top decision-makers. The success of this initiative was mainly due to Professors: Marian Grynborg, Jan Gaj, Jacek Kossut, and Tomasz Dietl, who prepared the organizational framework necessary to implement such an initiative. This is how the first Commissioned Research Project (Projekt Badawczy Zamawiany PBZ) *Physics and Technology of Low Dimensional Semiconductor Structures for Techniques of the Future Generation* (PBZ 101-15, 1993–1995) was born, which included, among others, tasks of purchasing and installing MBE and MOVPE reactors, as well as direct e-beam writer for patterning low-dimensional structures. This unprecedented effort has fundamentally changed the field of semiconductor physics and semiconductor optoelectronics in the country. In particular, one of the MBE reactors was installed at ITE (Fig. 10), and the e-beam writer — at the IF PAN premises.

5. Interinstitutional Laboratory of Nanostructures ITE–IF PAN

The first contacts between electronic engineers from ITE and physicists from IF PAN date back to the early 1970s, and the “Jaszowiec” Conferences were their constant element. Working at the



Fig. 11. The Laboratory of Nanostructures at IF PAN operated jointly with ITE, headed by Tomasz Dietl (IF PAN) and Anna Piotrowska (ITE).

same location and compatible disciplines fostered the exchange of knowledge and stimulated bilateral cooperation on a daily basis (Fig. 11). In the following years, the cooperation between teams from the Laboratory of Low Temperature Physics led by Tomasz Dietl, IP PAS, and the Department of III–V Semiconductor Structures ITE led by Anna Piotrowska gained particular importance. The joint project *Patterning of Quantum Wires and Dots by High Resolution e-beam Lithography*, lanced in the frame of PBZ 101-15, was an opportunity to deepen cooperation. The scope of the research activity involved: design and construction of a new clean room, commissioning of e-beam lithography facilities (JSM 6400 SEM equipped with Link's X-ray microprobe and a Raith pattern generator), development of basic lithography processes, as well as fabrication and characterization of II–VI and III–V 3D nanostructures, including CdTe, CdMnTe, HgCdMnTe, and GaAlAs/GaAs. The project was successfully completed and its scientific results made an important contribution to the general knowledge of properties and new physical phenomena. At the same time, it was evident that a coherent interinstitutional research group was established during the project, which would be worth giving a formal organizational framework. And this is how the Laboratory of Nanostructures was born. The agreement was signed on January 1, 1996, by Professor Henryk Szymczak (IP PAN) and Professor Cezary A. Ambroziak, directors of institutes. The document specified the rules of financing the laboratory and access to the shared infrastructure. Persons responsible for implementation of the agreement were Tomasz Dietl and Jerzy Wróbel (IF PAN) and Anna Piotrowska and Eliana Kamińska (ITE).

The cooperation turned out to be durable and valuable. The effect of synergy was clearly seen. The laboratory served scientists from other units of the institute, as well as from other research institutions.

6. ITE in a period of transformation and in the European Research Area

Two factors had a major impact on the activity of ITE during the transformation period, i.e., after the fall of communism. They were:

1. The degradation of the electronics industry in Poland in the late 1980s, in particular the collapse of the semiconductor fabrication plant TEWA, and the change in the rules of financing science.

In the absence of orders from industry and reduced grants from government programs, employment at ITE decreased by about 30%, and the silicon microelectronic line was moved to the Piaseczno Division. Individual departments of the Institute gained greater independence on the condition of obtaining appropriate funds.

2. The opportunity to access EU funds following Poland's accession to the European Union.

As a Newly Associated State, and then a full member, Poland could have its scientists participating in European research and technical programmes.

ITE actively participated, since 1994, in more than sixty projects within subsequent EC Framework Programmes and Concerted Actions. An important group of projects were those related to III–V and II–VI semiconductors, to name a few representative ones:

- Copernicus '95, the subject of which were tunable GaInAsSb/AlGaAsSb DH laser diodes for environmental pollutions control [45];
- VERTIGO — aimed at two-micron GaAs-based semiconductor disk lasers for gas sensing, communication and medical applications [46];
- WILD-EAST — related to InGaAs/GaAs laser diodes for Er-doped fibre amplifiers [47];
- AGETHA — targeting GaN-based amber/green resonant cavity LEDs, compatible with second-generation plastic optical fibre (POF) networks, able to operate at high temperatures and high data rates [48];
- TERAVISION — in which non-linear transmission line (NLTL) frequency multipliers based on heterostructure barrier varactors InGaAs/InAlAs were developed [49];
- AMORE — related to magnetism oxides [50];
- NANOPHOS — in which a number of oxide-based nanostructured photonics sensors was demonstrated [51];
- DENIS — focused on the development of monocrystalline GaN substrates for blue lasers [52];
- HYPHEN — targeted on SiC-based hybrid substrates for GaN-based high-frequency electronics [53],

- MORGAN — aimed to develop new solutions by exploiting the excellent physical properties of diamond and GaN-based heterostructures for electronic devices and sensors that could operate in extreme conditions, especially high temperatures, highly corrosive solutions, and strong electric fields [54].

ITE participated also in the R&D works of two Centres of Excellence:

- CEPHONA — headed by Professor Maciej Bugajski at ITE; research on the physics and technology of photonic nanostructures [55];
- CELDIS — headed by Professor Jacek Kossut at IF PAN; research on the physics and fabrication of low-dimensional compound semiconductor structures [56].

The achievements of ITE, which made a significant contribution to the implementation of the above-mentioned projects, included, among others:

- (i) development of major processing steps of InGaAsSb/AlGaAsSb DH mid-infrared laser diodes and photovoltaic detectors [57–64], e.g., surface preparation [57, 58], patterning mesa structures [59–61], formation of ohmic contacts [62–63], surface passivation [64];
- (ii) development and optimisation of processing steps for the fabrication of NLTTL structures, loaded with heterostructure barrier varactor (HBV) diodes InGaAs/InAlAs/AlAs/InAlAs/InGaAs [49], e.g., dry/wet etching, shaping HBV semiconductor material, formation of shallow ohmic contacts;
- (iii) fabrication of metal/oxide multilayer structures for interferometric studies and SnO₂ and ZnO diffractive elements for nanostructured gas sensors [65–68];
- (iv) novel approaches to the fabrication of ohmic contacts to GaN [69–80], e.g., n-type doping by creating nitrogen vacancies in the contact region of Ti-based metallizations [69], enhanced activation of the Mg acceptor to increase p-type doping of subcontact region of the ZrN/ZrB₂ ohmic contacts [70], n- and p-type doping via solid phase regrowth (SPR) for the ohmic contacts to n- and p-GaN [71, 72], engineering ZnO/GaN interface for the transparent ohmic contact to p-GaN [73, 74], engineering electronic structure of p-GaN surface via appropriate surface preparation procedure [75], advanced refractory metal-based metallizations with enhanced antidiffusion capabilities [76–80];
- (v) passivation of GaN-based heterostructures by a thin film of ZnO [81].

A research field with promising new applications in consumer electronics was amorphous oxide semiconductors. We demonstrated the possibility

to control the physicochemical properties of such amorphous oxide semiconductors as IGZO in a wide range by mastering the thin-film deposition parameters. By changing the reactive plasma composition and total deposition pressure, we can fabricate films with carrier concentration ranging from 10^{13} to 10^{20} cm⁻³, thus from highly resistive to highly conductive [82]. Using the ability to control the parameters of these oxide materials, we optimized the Schottky junction technology and used such rectifying contacts to fabricate transparent and flexible thin-film transistors in the MESFET (metal–semiconductor field-effect transistor) configuration at room temperature (RT). Furthermore, we demonstrated the possibility of using such devices in an innovative solution for glucose biodetection. By attaching glucose oxidase to the Schottky gate electrode of MESFET, the depletion area in the channel layer is modulated in proportion to the glucose concentration in the test solution [83].

In the first decade of 2000, several important investment projects were implemented. The largest of them was the creation of the Nanophotonics Center, including the launch of a complete technological line of III–V photonic devices, as well as the upgrade of the technological line of the Department of Micro and Nanotechnology of Wide-Break Semiconductors, including the purchase of a 3 MeV ion implanter equipped with RBS, ALD reactors, equipment for electron beam lithography and for nanoimprint.

Statutory research in the field of compound semiconductors has gone in two directions. The first one was III–V infrared photonics. The second one was wide-bandgap semiconductors for high frequency, high power and transparent electronics.

Among the works in the field of infrared photonics, a distinguishing achievement was the development of cascade laser technology, the description of which is presented in the next sections.

6.1. MBE at ITE. From single quantum well to quantum cascade lasers

Work on semiconductor lasers has been carried out at ITE since 1966. At the beginning, these were heterostructure lasers produced by liquid phase epitaxy. Significant progress was made in 1993 with the launch of a new technology of layer growth — epitaxy from molecular beams. The new technology allowed to begin work on a new generation of lasers based on low-dimensional structures, the so-called quantum well (QW) lasers. Quantum well lasers offer significant design flexibility and much improved performance compared to classical double heterostructure lasers. This paved the way for real telecommunication applications and led to intense research all over the world. We have been part of this emerging information technology (IT) market, contributing some application-oriented work on quantum well lasers.

All telecommunications-qualified 980 nm lasers are based on the ternary AlGaAs and InGaAs alloys of the AlGaInAs material system. The excellent lattice match, refractive index contrast, dopability, and thermal conductivity of AlGaAs give designers freedom to optimize the vertical structure, while the single pseudomorphic InGaAs quantum well active region provides high gain, good electrical confinement, and, therefore, low threshold current and high quantum efficiency.

Quantum well separate confinement heterostructure lasers (QW SCH) studied at ITE had a single quantum well (SQW) or multiple quantum well (MQW) active region. MQW active region leads to an effective increase of the electrically pumped volume and thus allows for high powers that are attractive for such applications as diode-pumped Nd:YAG lasers. However, the real driving force behind the development of quantum well lasers was telecommunications and data transmission technology. The development of erbium-doped fiber amplifiers (EDFA) has enabled the proliferation of high-bandwidth data networks. Er³⁺-doped fiber amplifiers coherently amplify 1550 nm signals through the conversion of 980 nm pump laser light. Because the process is entirely optical, many signals can be amplified simultaneously with no delay and with minimal electronics. The use of a pump wavelength of 980 nm has also another advantage, namely that no excited state absorption exists for this wavelength.

The technology of growth of 980 nm InGaAs/GaAs separate confinement heterostructure, single quantum well (SCH SQW) lasers has been developed for practical measures, based on our previous experiences with AlGaAs/GaAs semiconductor lasers fabricated at the Institute of Electron Technology [84, 85]. In the following, we will summarize the main results of work on 980 nm lasers [86]. A structure of a typical device is shown in Fig. 12. SCH SQW laser structures were grown by molecular beam epitaxy (MBE) in Riber 32P reactor. The structures were grown on (100) GaAs conductive substrates. The sequence of layers for a typical structure, optimized for reliable high power continuous wave (CW) operation, consisted of an n-type GaAs buffer, an Al_{0.3}Ga_{0.7}As n-type barrier layer, an undoped active layer and a waveguide, Al_{0.3}Ga_{0.7}As p-type barrier layer and p⁺-type GaAs subcontact layer. The active layer and the waveguide comprised of In_{0.21}Ga_{0.79}As 80 Å quantum well enclosed by 0.3 μm GaAs layers. The doping of both emitters was kept at $5 \times 10^{17} \text{ cm}^{-3}$ level.

Fabricated lasers exhibited threshold current densities of the order of $J_{th} \approx 280 \text{ A/cm}^2$ (for resonator length $L = 700 \text{ μm}$) and differential quantum efficiency $\mu = 0.40 \text{ W/A}$ (41%). The wall-plug efficiency of the lasers without AR/HR coating reached 38%. Optical power-current characteristics ($P-I$) for lasers fabricated from the same wafer

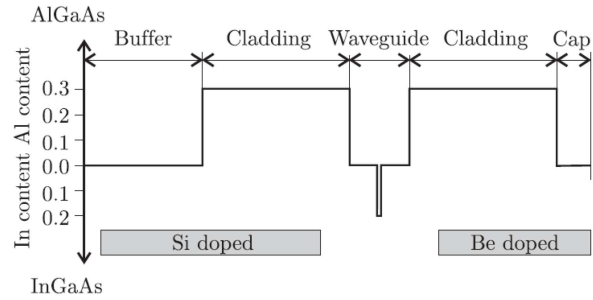


Fig. 12. SCH SQW InGaAs/GaAs strained layer laser structure.

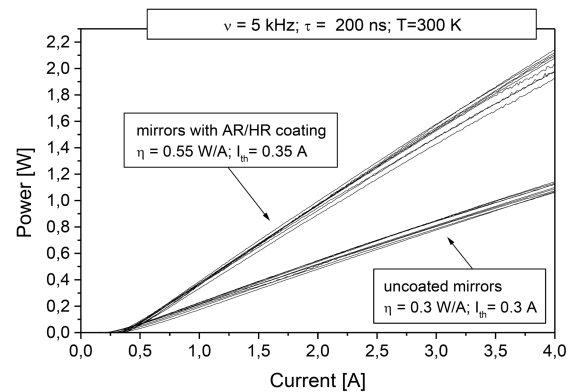


Fig. 13. Light-current ($L-I$) characteristics of the lasers with and without AR/HR facet coatings.

showed almost equal threshold and differential efficiency values. The linearity of the characteristics was good; no kinks and thermal roll-over were observed for the highest powers. The theoretical estimation of the threshold current density and differential efficiency obtained by numerical modeling of the devices were $J_{th} = 210 \text{ A/cm}^2$ and $\mu = 0.47 \text{ W/A}$, respectively. Typical light-current characteristics of lasers without AR/HR coatings and with AR/HR coatings, from one lot, are compared in Fig. 13. The threshold current of lasers with AR/HR coatings was unchanged compared to uncoated ones, but we have observed roughly two-fold increase in differential quantum efficiency. The record wall-plug efficiency for AR/HR coated devices was equal to 54%.

Aging tests proved generally good reliability of the lasers. The uncoated devices did not show significant degradation after over 1000 h of CW operation at a heat sink temperature of 35°C, with an emitted power of 50 mW (in a constant power mode). This result can be extrapolated to 10^6 h of pulse operation with $ff = 0.1\%$. Lasers with coated mirrors, operating at an aging frame in CW mode for 1500 h at constant power, maintained basically unchanged current, proving their applicable potential, even considering such demanding applications as the pump source for EDFA.

6.1.1. Quantum cascade lasers

The next major development was quantum cascade lasers (QCLs). We demonstrated them in 2009 [87]. Quantum cascade lasers are unipolar devices based on tunneling and intersubband transitions, in which the electronic states, wavefunctions and lifetimes of the relevant states are engineered through the quantum mechanical confinement imposed by the complex multilayer structure. The principle of operation of QCL structures places stringent requirements on the individual layer thickness and composition as well as the overall periodicity of the whole structure. Another crucial problem related to the QCL operation is the heating effect, which is distinctly larger than in the state-of-the-art bipolar lasers. Heating results in higher threshold and operation currents of the lasers, and all this, in turn, results in the necessity of effective heat extraction. Heat dissipation in QCLs is strongly hampered because of the nature of their active regions containing many interfaces and layers with a thickness close to the mean free path of phonons. QCLs are the major breakthrough in semiconductor laser technology, allowing to obtain a broad range of wavelengths from the infrared (IR) range of the spectrum by simply changing the geometry of the structure without the necessity of going to a different material system. Coherent sources in the mid-IR spectral range are of great interest due to the large number of applications in high-resolution molecular spectroscopy, industrial control and medical diagnostics. For the above reasons, over the last twenty five years, a big effort has been made to develop highly efficient quantum cascade lasers (QCLs) operating at this wavelength range. We will report here the major results of works on quantum cascade lasers at the Institute of Electron Technology. Technology of lasers, emitting at the wavelength ranges 9.0–9.5 μm and 4.7–5.25 μm , based on InGaAs/AlGaAs/GaAs and InAlAs/InGaAs/InP heterostructures; both lattice-matched and strain compensated has been developed [88–89].

6.1.2. GaAs based QCLs

The typical characteristics of $\text{Al}_{0.45}\text{Ga}_{0.55}\text{As}/\text{GaAs}$ ($\lambda=9.4 \mu\text{m}$) lasers developed at ITE are shown in Fig. 14.

6.1.3. InP based QCLs

The biggest drawback of mid-infrared GaAs-based QCLs results from the relatively low conduction band offset ($\sim 390 \text{ meV}$ for $\text{GaAs}/\text{Al}_{0.45}\text{Ga}_{0.55}\text{As}$) and carrier escape from the upper laser state to the continuum at elevated temperatures. This causes poor performance of GaAs/AlGaAs lasers at RT and excludes CW operation. Another consequence of the small band offset is the inability to move emission to shorter wavelength, in particular in the range of $\sim 4\text{--}5 \mu\text{m}$, which is interesting from the point of view of

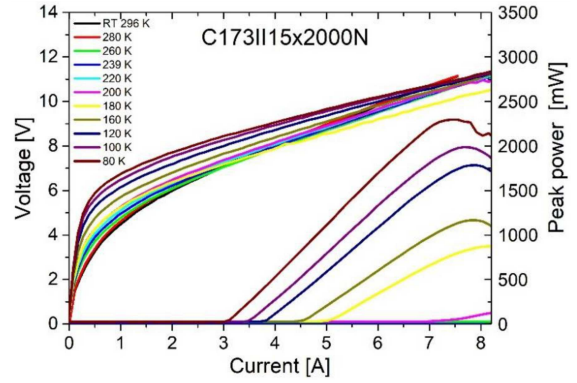


Fig. 14. Light-current and current-voltage (L - I - V) characteristics of the $\text{Al}_{0.45}\text{Ga}_{0.55}\text{As}/\text{GaAs}$ ($\lambda = 9.4 \mu\text{m}$) laser with uncoated facets, driven by 200 ns pulses with repetition rate 5 kHz. The laser cavity length equals 2 mm and the mesa width equals 15 μm .

applications in molecular spectroscopy. The rule of thumb is that the band offset should be roughly three times the emission energy ($\Delta E \approx 3h\nu$) to properly nest the lower and upper laser levels in quantum wells. The problem can be solved by using InGaAs/InAlAs/InP structures which offer much higher band offset, i.e., $\sim 520 \text{ meV}$ in the case of lattice-matched heterostructures and up to 800 meV in the case of strain-compensated heterostructures. The price one pays, however, is greatly increased technological complexity. The material system is based on two ternary compounds (InAlAs/InGaAs), which are not lattice-matched to InP for all possible compositions except one. This requires a high growth precision in terms of composition and makes the analysis of heterostructure parameters more difficult. Additionally, in strain-compensated structures, it is necessary to control the compositions of four different ternary alloys in the waveguide and active region during growth.

AlInAs/GaInAs/InP heterostructures were used for the construction of a short wavelength laser emitting at around 5 μm . This was done by taking advantage of the modification of the band structure of ternaries AlInAs and GaInAs caused by strain. $\text{Ga}_{0.467}\text{In}_{0.533}\text{As}/\text{Al}_{0.477}\text{In}_{0.523}\text{As}/\text{InP}$ heterostructure is lattice-matched to InP. When the composition of ternaries deviates from the above, the individual layers undergo biaxial deformation in the plane perpendicular to the direction of growth. Tensile strain in AlInAs barriers moves the conduction band edge to higher energies, whereas compressive strain in InGaAs wells moves the conduction band edge in the opposite direction. As a result, the conduction band offset in the AlInAs/GaInAs heterostructure increases. An example of such structure is $\text{Ga}_{0.331}\text{In}_{0.669}\text{As}/\text{Al}_{0.638}\text{In}_{0.362}\text{As}$, for which the conduction band offset is $\sim 800 \text{ meV}$.

TABLE II

Parameters of the lattice-matched and strain-compensated AlInAs/In₀GaAs/InP lasers: J_{th} [kA/cm²] — threshold current density, V_{th} [V] — threshold voltage, T_0 [K] and T_1 [K] — characteristic temperatures, and η [W/A] — maximum slope efficiency.

Parameter	Lattice-matched QCL		Strain-compensated QCL	
	MBE	MBE + MOVPE	MBE	MBE + MOVPE
J_{th} (77 K) [$\frac{kA}{cm^2}$]	2.15	1.5	1.05	0.91
J_{th} (295 K) [$\frac{kA}{cm^2}$]	4.6	3.3	3.3	2.3
V_{th} (77 K) [V]	10.3	7.8	20.6	15.1
V_{th} (295 K) [V]	10.4	6.7	19.3	12.9
T_0 [K]	135	170	128	154
T_1 [K]	136	196	204	208
η [W/A]	0.69	1.19	0.61	2.27

In such a case, despite the $\sim 1\%$ lattice mismatch of individual layers, the global strain is balanced and we are dealing with pseudomorphic growth of the whole laser structure. One has to note, however, that the growth of such structures is the ultimate challenge for MBE. The L - I - V characteristics of the strain-compensated InGaAs/InAlAs/InP ($\lambda = 4.7 \mu\text{m}$) lasers developed at ITE are shown in Fig. 15. Parameters of the lattice-matched and strain-compensated AlInAs/In₀GaAs/InP lasers are summarized in Table II.

Technology of quantum cascade lasers, emitting at the wavelengths 9.0–9.5 μm and 4.7 μm , is based on InGaAs/AlGaAs/GaAs and InAlAs/InGaAs/InP heterostructures; both lattice-matched and strain-compensated ones have been developed. The structures were grown by MBE and by MOVPE. InGaAs/AlGaAs/GaAs lasers were grown by MBE. For InP-based lasers, three types of structures were investigated: the one grown exclusively by MBE without MOVPE overgrowth, the remaining two fabricated by hybrid approach combining the MBE-grown InAlAs/InGaAs active region with the MOVPE-grown InP waveguide. All presented types of lasers had parameters typical for the design, thanks to which the laser were successfully tested in prototype gas detection systems and free-space communication systems.

6.2. Microwave AlGaIn/GaN high electron mobility transistors (HEMTs) on truly semi-insulating GaN substrates

Work on GaN-based devices was carried out at ITE from the mid-1990s of the last century. At that time, only a limited number of research laboratories was capable to grow high-quality n-type and p-type epitaxial material. Owing to bilateral scientific cooperation with US laboratories, our first research was performed on epitaxial films from North Carolina State University and Xerox Palo Alto Research Center (PARC)

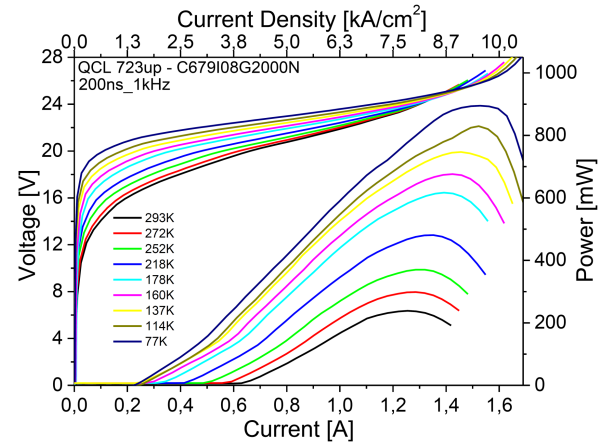


Fig. 15. The L - I - V characteristics of the strain-compensated InGaAs/InAlAs/InP ($\lambda = 4.7 \mu\text{m}$) lasers developed at ITE.

Electronic Materials Laboratories [69, 70]. Soon we could work on GaN-based heterostructures fabricated in European laboratories participating in European projects. At the same time, cooperation with research groups in the country was initiated. The turning point for further activities was the launch of 2" n-type monocrystalline GaN substrates by Ammono S.A., which created an opportunity to improve the quality of epitaxial structures and increase the reliability of the devices. Bearing in mind potential end-users, the aim of the work was the microwave AlGaIn/GaN HEMT transistor for the S-band. The complete value chain was set up in the frame of cooperative project PoHEMT [90] by the consortia including Ammono S.A., responsible for the development of semi-insulating GaN substrate, the Institute of High Pressures PAS and TopGaN Ltd working on MOCVD growth and characterisation of AlGaIn/GaN structures, the Institute of Physics PAS targeting AlGaIn/GaN MBE growth, the Institute of Electron Technology (project leader) developing processing of HEMT

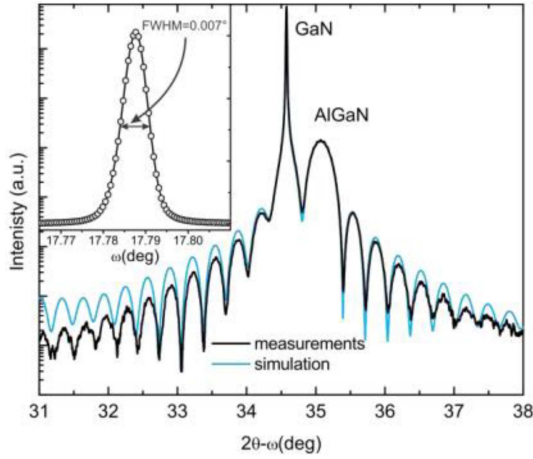


Fig. 16. The $2\theta-\omega$ high-resolution XRD scan of the MOCVD-grown AlGaIn/GaN HEMT structure on the SI Ammono-GaN substrate [91].

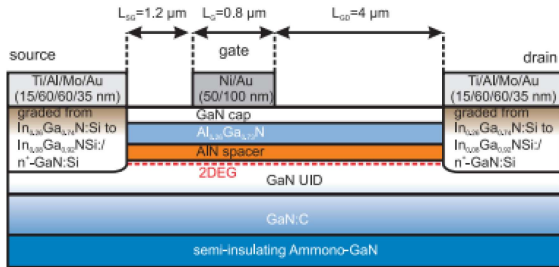


Fig. 17. Cross-sectional diagram of AlGaIn/GaN-on-Ammono GaN HEMT with regrown GaN/InGaIn graded composition epitaxial bilayer [91].

structures, the Institute of Radioelectronics and Multimedia Techniques of Warsaw University of Technology performing radio-frequency (RF) characterisation and reliability testing.

Next, the 1,5" semi-insulating (SI) Ammono-GaN substrates characterised by the FWHM values of X-ray rocking curve of about 20 arcsec, a curvature radius of c -planes of several tens of meters, and dislocation density below $5 \times 10^4 \text{ cm}^{-2}$, have been developed. Their room temperature resistivity was typically no less than $10^9 \Omega \text{ cm}$ as measured by the frequency domain capacitive technique (with electric field \parallel to c -axis), and over $1 \times 10^6 \Omega \text{ cm}$ as measured by the microwave methods (above the measurement method range, electric field \perp to c -axis). The thermal conductivity was $\sim 230 \text{ W/(m K)}$ at RT. Of crucial importance for optimizing the growth of highly resistive GaN substrates was the suppression of oxygen content below $2 \times 10^{18} \text{ cm}^{-3}$ and the choice of appropriate acceptors for compensating residual native donors.

AlGaIn/GaN HEMT structures grown by MOCVD method consisted of 1 nm GaN-cap, 25 nm $\text{Al}_{0.26}\text{Ga}_{0.74}\text{N}$ barrier layer, 0.8 nm AlN

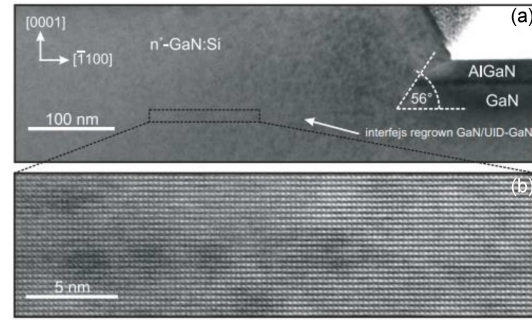


Fig. 18. (a) TEM image of $n^+\text{In}_x\text{Ga}_{1-x}\text{N}:\text{Si}/n^+\text{GaN}:\text{Si}$ region and (b) HRTEM (high-resolution transmission electron microscopy) image of $n^+\text{GaN}:\text{Si}/\text{UID}$ GaN interface [91].

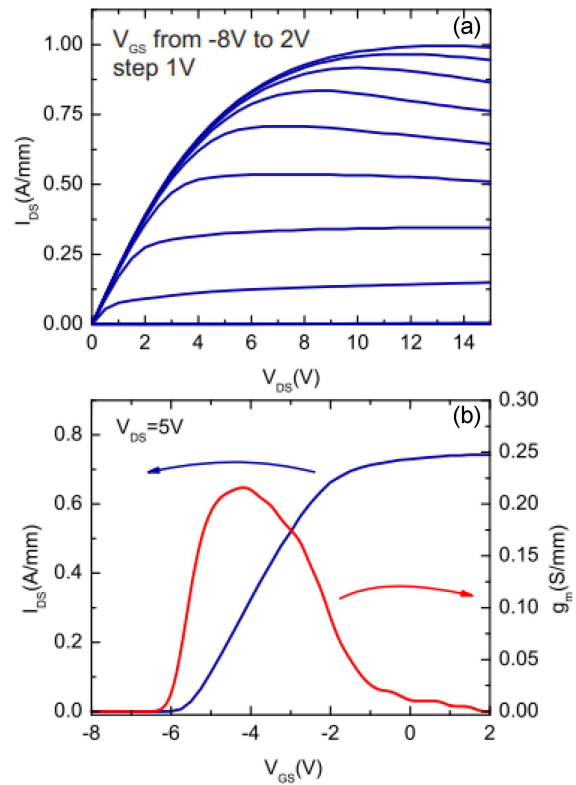


Fig. 19. (a) Output and (b) transfer characteristics of AlGaIn/GaN HEMT on semi-insulating Ammono-GaN [91].

spacer, $0.7 \mu\text{m}$ unintentionally doped GaN layer, and $1 \mu\text{m}$ highly resistive GaN:C buffer. A special process was developed to prevent decomposition of the N-face backside of the substrate during high-temperature MOCVD growth. The high resolution $2\theta-\omega$ rocking curve scan (Fig. 16) proves the excellent crystal quality of epilayers grown on Ammono-GaN with $\text{FWHM} = 0.007^\circ$. The AFM images showed atomically smooth surface with a root mean square roughness of about 0.12–0.14 nm. The electrical parameters of the two-dimensional

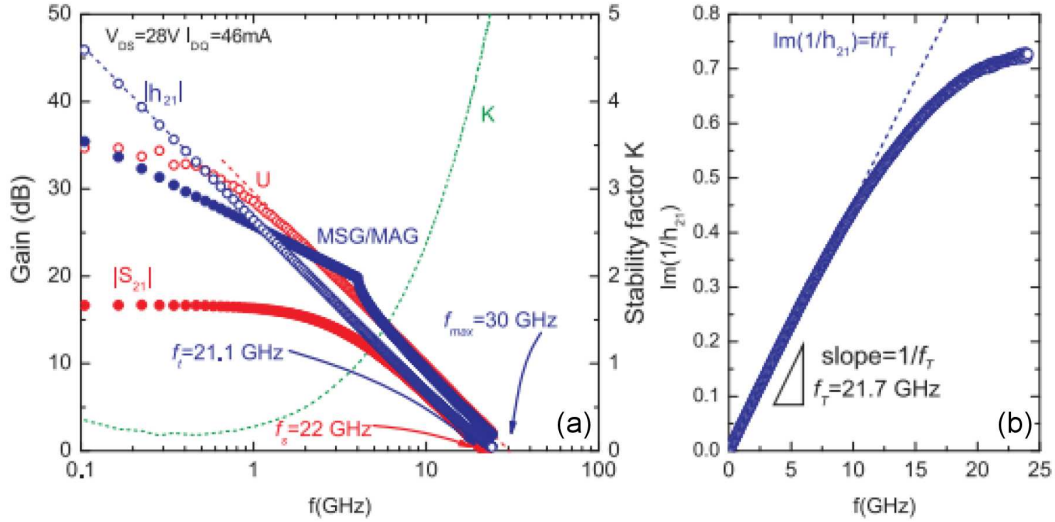


Fig. 20. (a) High-frequency characteristics of $|S_{21}|$, $|h_{21}|$, U and MSG/MAG AlGaIn/GaN HEMT on semi-insulating Ammono-GaN. (b) Determination of f_T by the Gummel method [91].

electron gas (2DEG) as measured by the Hall effect in Van der Pauw geometry were as follows: sheet carrier concentration $n_s = 1.64 \times 10^{13} \text{ cm}^{-2}$, Hall mobility $\mu_H = 1210 \text{ cm}^2/(\text{V s})$, sheet resistivity $R_{sh} = 315 \Omega/\square$.

Figure 17 shows a scheme of the HEMT device structure. The gate length L_G was $0.8 \mu\text{m}$, the source to gate L_{SG} and gate to drain L_{GD} distances were $1.2 \mu\text{m}$ and $4 \mu\text{m}$, respectively.

The main processing steps included the formation of source and drain ohmic contacts, isolation of adjacent HEMT structures, formation of gate contacts, passivation of HEMT devices, making electrical beam leads [91, 92]. Out of a number of approaches undertaken to make low-resistance ohmic contacts, the best was to grow additional highly-doped lower-bandgap nitride $n^+\text{In}_x\text{Ga}_{1-x}\text{N}:\text{Si}/n^+\text{GaN}:\text{Si}$ regrow bilayer below the source and drain metallization. The depth of recess was 20 nm below the AlGaIn barrier layer, the composition of $n^+\text{In}_x\text{Ga}_{1-x}\text{N}:\text{Si}$ gradually varied from 8 at.% to 26 at.% at the top. Figure 18 depicts TEM images of the regrown semiconductor contact regions, showing the high crystal quality of regrown $n^+\text{GaIn}$ layer and the smooth $n^+\text{GaIn}/\text{UID GaIn}$ interface. The etched sidewalls are at an angle of 56° to the c -plane (0001). The sidewall angle is close to the optimal angle of 62° at which the density of dangling bonds on the etched surface is similar to the c -plane surface. Heat-treated Ti/Al/Mo/Au metallization enabled achieving ohmic contacts with a resistance of $R_c = 0.43 \Omega \text{ mm}$ and a resistivity of $\rho_c = 6.4 \times 10^{-6} \Omega \text{ cm}^2$.

Isolation of adjacent HEMT devices was done by using two-step Al⁺ ion implantation [93, 94]. The first step was with an energy 800 keV and a dose $1.5 \times 10^{13} \text{ cm}^{-2}$, and the second with an energy 300 keV and dose $1 \times 10^{13} \text{ cm}^{-2}$. The sheet

resistivity of implanted isolation was $10^{11} \Omega/\square$, and the depth of isolation was $0.7 \mu\text{m}$. Electron-beam deposited Ni/Au bilayers were used for gate electrodes, while the SiN_x overcoat was applied for device passivation.

The output and transfer characteristics of AlGaIn/GaN HEMTs are depicted in Fig. 19. The maximum output current density reaches 1000 mA/mm at $V_{GS} = 2 \text{ V}$. The extracted on-state resistance R_{on} was about $4.4 \Omega/\text{mm}$. The transfer characteristics show a clear pinch-off at $V_{GS} = -6 \text{ V}$. The transistor transconductance exceeded 220 mS and reached the maximum value for the expected range of operating points of the transistors. No measurable leakage current was observed across the buffer layers or the substrate. The high-frequency performances of transistors, evaluated by measuring on-wafer the S -matrix parameters over the frequency range from 45 MHz to 24 GHz at the operating point V_{DSQ} and I_{DSQ} , are shown in Fig. 20a, which displays the characteristics of the insertion gain $|S_{21}|$ and the ratio MSG/MAG, read as maximum stable gain/maximum available gain. The frequency f_{MAG} defined for MSG/MAG = 0 dB amounted to 31 GHz . The cut-off frequency value, f_T , obtained by linear extrapolation, with -20 dB/dec slope of the small signal current gain, was 21.7 GHz (see Fig. 20b). The insertion gain $|S_{21}|$ was equal to 0 dB for a frequency $f_s = 22 \text{ GHz}$. In the S -band, the maximum available gain was 22.7 dB and 19.8 dB at 2 GHz and 4 GHz , respectively, whereas the small signal gain was 15.3 dB and 12.7 dB within the same respective frequency range. The high potential of the developed technology was proved by assembling the obtained devices in S -band power amplifiers, which achieved the maximum power density of 4.15 W/mm .

Overall, AlGaIn/GaN-on-Ammono GaN HEMTs compare well with devices manufactures on silicon carbide substrates available from commercial manufacturers. This also applies to their thermal parameters [95].

7. Epilogue

The year 2019 opened a new chapter in the history of the Institute of Electron Technology. On April 1, ITE became part of the newly established Łukasiewicz Research Network (SBL). A year later, on October 1, 2020, the Institute was merged with the Institute of Electronic Materials Technology SBL establishing the Institute of Microelectronics and Photonics. The description of the Institute activity is regularly displayed on its website.

References

- [1] J. Kubiawski, *Sylwetki Profesorów Politechniki Warszawskiej, Janusz Groszkowski (1898–1984)*.
- [2] *Bohdan Paszkowski (1915–2000)*, Instytut Mikroelektroniki i Optoelektroniki PW.
- [3] Witold Rosiński — Nestor Polskiej Elektroniki Sam o Sobie.
- [4] J. Klamka, E. Kuźma, J. Pułtorak, S. Sikorski, E. Stolarski, J. Świdorski, *Prace ITE* **1992** z. 8, 3 (1992).
- [5] B. Mroziewicz, J. Świdorski, B. Darek, *Arch. Elektrotechniki* **15**, 165 (1966).
- [6] B. Mroziewicz, P. Dąbrowski, *Przegląd Elektrotechniczny* **8**, 535 (1966).
- [7] S.A. Ignatowicz, *Thin Solid Films* **6**, 299 (1970).
- [8] A. Piotrowska, *Thin Solid Films* **24**, 143 (1974).
- [9] A. Piotrowska, E. Mizera, *Thin Solid Films* **44**, 305 (1977).
- [10] S.A. Ignatowicz, A. Dajna, Z. Goliger, A. Mikułko, A. Piotrowska, *Thin Solid Films* **36**, 399 (1976).
- [11] A. Dajna, A. Mikułko, A. Piotrowska, *Elektronika* **17**, 444 (1976).
- [12] A. Dajna, A. Mikułko, A. Piotrowska, *Pomiary Automatyka Kontrola* **XXIII**, 32 (1977).
- [13] A. Piotrowska, B. Mroziewicz, *Elektronika* **XXVII**, 9 (1986).
- [14] B. Mroziewicz, *50 lat Instytutu Technologii Elektronowej 1966–2016*, Eds. Elektronowej, J. Kaniewski, B. Mroziewicz, A. Piotrowska, Instytut Technologii, Warszawa 2017, p. 11.
- [15] A. Piotrowska, A. Guivarc’h, G. Pelous, *Solid State Electron.* **26**, 179 (1983).
- [16] A. Piotrowska, E. Kaminska, *Rozprawy Elektrotechniczne* **32**, 545 (1986).
- [17] A. Piotrowska, E. Kaminska, *Thin Solid Films* **193/194**, 511 (1990).
- [18] A. Piotrowska, *Acta Phys. Pol. A* **84**, 491 (1993).
- [19] A. Barcz, E. Kaminska, A. Piotrowska, *Thin Solid Films* **149**, 251 (1987).
- [20] A. Piotrowska, E. Kaminska, A. Barcz, J. Adamczewska, A. Turows, *Thin Solid Films* **130**, 231 (1985).
- [21] X.W. Lin, Z. Liliental-Weber, J. Washburn, A. Piotrowska, E. Kamińska, *Mater. Res. Soc. Symp. Proc.* **260**, 469 (1992).
- [22] A. Piotrowska, E. Kamińska, S. Kwiatkowski, A. Turows, *J. Appl. Phys.* **73**, 4404 (1993).
- [23] X.W. Lin, Z. Liliental-Weber, J. Washburn, A. Piotrowska, E. Kamińska, *J. Vac. Sci. Technol. B* **11**, 44 (1993).
- [24] E. Kamińska, A. Piotrowska, J. Adamczewska, R. Żarecka, E. Mizera, *Mater. Res. Soc. Symp. Proc.* **300**, 237 (1993).
- [25] A. Piotrowska, E. Kamińska, X.W. Lin, Z. Liliental-Weber, J. Washburn, E. Weber, S. Gierlotka, J. Adamczewska, S. Kwiatkowski, A. Turows, *J. Vac. Sci. Technol. B* **11**, 572 (1993).
- [26] X.W. Lin, A. Piotrowska, E. Kaminska, Z. Liliental-Weber, J. Washburn, E. Weber, *Appl. Phys. Lett.* **62**, 2995 (1993).
- [27] X.W. Lin, A. Piotrowska, E. Kaminska, Z. Liliental-Weber, J. Washburn, *Mater. Res. Soc. Symp. Proc.* **300**, 285 (1993).
- [28] A. Piotrowska, E. Kamińska, X.W. Lin, Z. Liliental-Weber, J. Washburn, E. Weber, A. Barcz, S. Gierlotka, S. Kwiatkowski, *Opto-Electron. Rev.* **3**, 72 (1993).
- [29] E. Kaminska, A. Piotrowska, E. Mizera, E. Dynowska, *Thin Solid Films* **246**, 143 (1994).
- [30] A. Piotrowska, E. Kamińska, M. Guzewicz, S. Kwiatkowski, A. Turows, *Mater. Res. Soc. Symp. Proc.* **300**, 219 (1993).
- [31] E. Kamińska, A. Piotrowska, E. Mizera, M. Guzewicz, A. Barcz, E. Dynowska, S. Kwiatkowski, *Mater. Res. Soc. Symp. Proc.* **337**, 349 (1994).
- [32] A. Piotrowska, E. Kamińska, M. Guzewicz, T. Piotrowski, S. Kwiatkowski, *Mater. Res. Soc. Symp. Proc.* **342**, 137 (1994).
- [33] M. Guzewicz, A. Piotrowska, E. Kamińska, E. Mizera, K. Gołaszewska, A. Turows, A. Winiarski, J. Szade, *Solid State Electron.* **43**, 1055 (1999).

- [34] M. Guziewicz, Ph.D. Thesis, Instytut Technologii Elektronowej, 2000.
- [35] A.V. Kuchuk, V.P. Kladko, V.F. Machulin, A. Piotrowska, E. Kamińska, K. Gołaszewska, R. Ratajczak, R. Minikauiev, *Rev. Adv. Mater. Sci.* **8**, 22 (2004).
- [36] A. Kuchuk, E. Kamińska, A. Piotrowska, K. Gołaszewska, E. Dynowska, O.S. Lytvyn, L. Nowicki, J. Ratajczak, *Thin Solid Films* **459**, 292 (2004).
- [37] A. Piotrowska, P. Auvray, A. Guivarc'h, G. Pelous, P. Henoc, *J. Appl. Phys.* **52**, 5112 (1981).
- [38] A. Piotrowska, P. Auvray, G. Guenais, A. Guivarc'h, G. Pelous, P. Henoc, *Electron. Technol.* **15**, 13 (1982).
- [39] E. Kamińska, A. Piotrowska, A. Barcz, J. Adamczewska, A. Turows, *Solid State Electron.* **29**, 279 (1986).
- [40] A. Piotrowska, E. Kamińska, M. Guziewicz, R. Veresegyhazy, I. Mojzes, B. Pecz, *Acta Phys. Pol. A* **80**, 457 (1991).
- [41] A. Piotrowska, E. Kamińska, M. Guziewicz, E. Mizera, E. Dynowska, X.W. Lin, S. Rouvimov, Z. Liliental-Weber, S. Kwiatkowski, *Mater. Res. Soc. Symp. Proc.* **403**, 669 (1996).
- [42] E. Kamińska, A. Piotrowska, M. Guziewicz, K. Gołaszewska, A. Barcz, A. Turows, E. Mizera, J. Adamczewska, S. Rouvimov, Z. Liliental-Weber, M.D. Bremser, R.F. Davis, *Electron. Technol.* **32**, 304 (1999).
- [43] S. Mackowski, Nguyen The Koi, A. Golnik, P. Kossacki, J.A. Gaj, E. Kamińska, A. Piotrowska, G. Karczewski, T. Wojtowicz, J. Kossut, *Solid State Commun.* **107**, 267 (1998).
- [44] M. Guziewicz, E. Kamińska, "Metalizacja do Półprzewodnikowych Materiałów Elektronicznych na Bazie PbTe oraz Sposób Wykonania tej Metalizacji", Polish Patent no. P3999296.
- [45] Control of Environmental Pollutions by Tunable Laser Absorption Spectroscopy in the spectral Range 2–4 μ m, Copernicus'95, ID: CIPA-CT-0158.
- [46] Versatile Two Micron Light Source, VERTIGO FP6-IST, ID: 034692.
- [47] Wide Aperture Coherent Laser Diodes for Erbium Doped Fibre Amplifiers, WILD-EAST, FP5-IST ID: 1999-10787.
- [48] Amber/Green Emitters Targeting High Temperature Applications, AGETHA, FP5-IST ID: 1999-10292.
- [49] Terahertz Frequency Imaging systems for Biomedical and other Applications, TERAVISION FP5-IST, ID: 1999-101154.
- [50] Advanced Magnetic Oxides for Responsive Engineering, AMORE, FP5-GROWTH, ID: G5RD-CT-2000-00138.
- [51] Nanostructured Photonic Sensors, NANOPHOS, FP5 ID: IST-2001-39112.
- [52] Development of Low Dislocation Density GaN Substrates, DENIS, FP5, ID: G5RD-CT-2001-00566.
- [53] Hybrid Substrates for Competitive High Frequency Electronics, HYPHEN, FP6, IST, ID: 027456.
- [54] Materials for Robust Gallium Nitride, MORGAN, FP7, Growth, ID: 24161.
- [55] Physics and Technology of Photonic Nanostructures, CEPHONA, Centre of Excellence, FP5-GROWTH, ID: G5MA-CT-2002-04061.
- [56] Physics & Fabrication of Low-Dimensional Structures for Technologies of Future Generations, Institute of Physics, FP5-GROWTH, ID: ICA1-CT-2000-70018.
- [57] A. Piotrowska, E. Kamińska, T.T. Piotrowski, M. Piskorski, M. Guziewicz, E. Papis, K. Gołaszewska-Malec, S. Kasjaniuk, *Acta Phys. Pol. A* **90**, 903 (1996).
- [58] E. Papis-Polakowska, Ph.D. Thesis, Instytut Technologii Elektronowej, 2004.
- [59] A. Piotrowska, M. Guziewicz, E. Kamińska, E. Papis, *Mater. Res. Soc. Symp. Proc.* **450**, 67 (1997).
- [60] T.T. Piotrowski, E. Papis, M. Guziewicz, K. Gołaszewska, E. Kamińska, A. Piotrowska, I.A. Andreev, M.P. Mikhailova, E.V. Kunitsyna, Yu. P. Yakovlev, *Electron. Technol.* **31**, 304 (1998).
- [61] A. Piotrowska, E. Kamińska, T.T. Piotrowski, M. Guziewicz, K. Gołaszewska, E. Papis, J. Wróbel, L. Perchuć, *Vacuum* **56**, 57 (2000).
- [62] M. Guziewicz, A. Piotrowska, T.T. Piotrowski, K. Gołaszewska, L. Ilka, I. Wójcik, J. Kątcki, A. Łaszcz, R. Mogilinski, J. Nowinski, R. Ratajczak, *Proc. SPIE* **5136**, 187 (2003).
- [63] T.T. Piotrowski, A. Piotrowska, E. Kamińska, K. Gołaszewska, E. Papis, M. Piskorski, W. Jung, J. Kątcki, A. Kudła, J. Adamczewska, J. Piotrowski, Z. Nowak, Z. Orman, J. Pawluczyk, *Mater. Res. Soc. Symp. Proc.* **607**, 89 (2000).
- [64] A. Piotrowska, E. Papis, K. Gołaszewska, R. Łukasiewicz, E. Kamińska, T.T. Piotrowski, R. Kruszka, A. Dudła, J. Rutkowski, J. Szade, A. Winiarski, A. Wawro, M. Aleszkiewicz, *Mater. Res. Soc. Symp. Proc.* **829**, B6.8.1 (2005).

- [65] E. Kamińska, A. Piotrowska, J. Kossut, R. Butkute, W. Dobrowolski, K. Gołaszewska, A. Barcz, R. Jakiela, E. Dynowska, E. Przeździecka, D. Wawer, *Mater. Res. Soc. Symp. Proc.* **786**, E6.1.1 (2004).
- [66] E. Kamińska, A. Piotrowska, J. Kossut, R. Butke, W. Dobrowolski, R. Łukasiewicz, A. Barcz, R. Jakiela, E. Dynowska, E. Przeździecka, M. Aleszkiewicz, P. Wojnar, E. Kowalczyk, *Phys. Stat. Sol. (c)* **2**, 1119 (2005).
- [67] E. Kaminska, A. Piotrowska, J. Kossut, A. Barcz, R. Butke, W. Dobrowolski, E. Dynowska, R. Jakiela, E. Przeździecka, R. Łukasiewicz, M. Aleszkiewicz, P. Wojnar, E. Kowalczyk, *Solid. State Commun.* **135**, 11 (2005).
- [68] E. Kaminska, E. Przeździecka, A. Piotrowska, J. Kossut, E. Dynowska, W. Dobrowolski, A. Barcz, R. Jakiela, E. Łusakowska, J. Ratajczak, *Mater. Res. Soc. Symp. Proc.* **786**, EE08-11.1 (2005).
- [69] E. Kaminska, A. Piotrowska, M. Guziewicz, S. Kasjaniuk, A. Barcz, E. Dynowska, M.D. Bremser, O.H. Nam, R.F. Davis, *Mater. Res. Soc. Symp. Proc.* **449**, 1055 (1997).
- [70] E. Kaminska, A. Piotrowska, A. Barcz, D. Bour, M. Zielinski, J. Jasinski, *Mater. Sci. Eng. B* **82**, 265 (2001).
- [71] E. Kamińska, A. Piotrowska, J. Jasiński, J. Kozubowski, A. Barcz, K. Gołaszewska, D.B. Thomson, R.F. Davis, M.D. Bremser, *Mater. Res. Soc. Internet J. Nitride Semicond. Res.* **4S1**, G9.9 (1998).
- [72] E. Kamińska, A. Piotrowska, A. Barcz, M. Guziewicz, S. Kasjaniuk, M.D. Bremser, R.F. Davis, E. Dynowska, S. Kwiatkowski, *Mater. Res. Soc. Symp. Proc.* **482**, 1077 (1998).
- [73] E. Kaminska, A. Piotrowska, K. Gołaszewska, A. Barcz, R. Kruszka, T. Ochalski, J. Jasiński, Z. Liliental-Weber, *Phys. Status Solidi (c)* **0**, 231 (2002).
- [74] E. Kaminska, A. Piotrowska, K. Gołaszewska, R. Kruszka, A. Kuchuk, J. Szade, A. Winiarski, J. Jasiński, Z. Liliental-Weber, *J. Alloys Compd.* **371**, 129 (2004).
- [75] E. Kaminska, A. Piotrowska, K. Gołaszewska, R. Łukasiewicz, A. Szczesny, E. Kowalczyk, P. Jagodzinski, M. Guziewicz, A. Kudła, A. Barcz, R. Jakiela, *Mater. Res. Soc. Symp. Proc.* **831**, E3.41.1 (2005).
- [76] J. Jasinski, E. Kaminska, A. Piotrowska, A. Barcz, M. Zielinski, *Mater. Res. Soc. Symp. Proc.* **622**, T6.34.1 (2000).
- [77] E. Kaminska, K. Gołaszewska, A. Piotrowska, A. Kuchuk, R. Kruszka, E. Papis, R. Szeloch, P. Janus, T. Gotszalk, A. Barcz, *Phys. Status Solidi (c)* **1**, 219 (2004).
- [78] A. Piotrowska, E. Kamińska, M. Guziewicz, E. Dynowska, A. Stonert, A. Turos, S. Figge, R. Kröger, D. Hommel, *Mater. Res. Soc. Symp. Proc.* **892**, 0892-FF14-05.1 (2006).
- [79] E. Kaminska, I. Pasternak, M. Borysiewicz, M. Guziewicz, A. Piotrowska, E. Dynowska, R. Jakiela, V. Kolkovski, M.-A. di Forte-Poisson, *Mater. Res. Soc. Online Proc. Lib.* **1298**, 233 (2011).
- [80] M.A. Borysiewicz, E. Kaminska, M. Mysliwiec, M. Wzorek, A. Kuchuk, A. Barcz, E. Dynowska, M.-A. di Forte-Poisson, C. Giessen, A. Piotrowska, *J. Cryst. Res. Technol.* **3**, 261 (2012).
- [81] E. Kaminska, A. Piotrowska, M.-A. di Forte Poisson, S. Delage, H. Lahreche, N. Kwietniewski I. Pasternak, R. Kruszka, M. Guziewicz, P. Bogusławski, E. Dynowska, M. Borysiewicz, *Mater. Res. Soc. Symp. Proc.* **1035**, L08-08 (2008).
- [82] T. Boll, M. A. Borysiewicz, A. Taube, M. Thuvander, J.-Y. Law, E. Kaminska, K. Stiller, *Thin Solid Films* **608**, 57 (2016).
- [83] J. Kaczmarek, J. Jankowska-Śliwińska, M.A. Borysiewicz, *Jpn. J. Appl. Phys.* **58**, 090603 (2019).
- [84] M. Bugajski, M. Kaniewska, K. Regiński, J. Muszalski, D. Kryńska, A. Litkowiec, *Electron Technol.* **29**, 346 (1996).
- [85] M. Bugajski, M. Kaniewska, K. Regiński, A. Małąg, S. Łepkowski, J. Muszalski, *Proc. SPIE* **3186**, 310 (1997).
- [86] M. Bugajski, B. Mroziejewicz, K. Regiński, J. Muszalski, K. Kosiel, M. Zbrozarczyk, T. Ochalski, T. Piwoński, D. Wawer, A. Szerling, E. Kowalczyk, H. Wrzesińska, M. Górka, *Bull. Pol. Acad. Sci. Technic. Sci.* **53**, 113 (2005).
- [87] K. Kosiel, M. Bugajski, A. Szerling, J. Kubacka-Traczyk, P. Karbownik, E. Pruszyńska-Karbownik, J. Muszalski, A. Łaszcz, P. Romanowski, M. Wasiak, W. Nakwaski, I. Makarowa, P. Perlin, *Photon. Lett. Pol.* **1**, 16 (2009).

- [88] M. Bugajski, P. Gutowski, P. Karbownik, A. Kolek, G. Hałdaś, K. Pierściński, D. Pierścińska, J. Kubacka-Traczyk, I. Sankowska, A. Trajnerowicz, K. Kosiel, A. Szerling, *Phys. Status Solidi (b)* **251**, 1144 (2014).
- [89] M. Bugajski, D. Pierścińska, P. Gutowski, K. Pierściński, G. Sobczak, K. Janus, I. Sankowska, K. Michalak, K. Chmielewski, J. Branias, A. Kuźmich, *Proc. SPIE* **10974**, 1 (2018).
- [90] Tranzystory Mikrofalowe HEMT Al-GaN/GaN na Monokrystalicznych Podłożach GaN PolHEM, Projekt Badawczy Zamawiany (PBZ), PBS1/A3/9/2012.
- [91] A. Piotrowska, E. Kamińska, W. Wojtasiak, W. Gwarek, R. Kucharski, M. Zająć, P. Prystawko, P. Kruszewski, M. Ekielski, J. Kaczmarek, M. Kozubal, A. Trajnerowicz, A. Taube, *ECS Transactions* **75**, 77 (2016).
- [92] W. Wojtasiak, M. Góralczyk, D. Gryglewski, M. Zajac, R. Kucharski, P. Prystawko, A. Piotrowska, M. Ekielski, E. Kamińska, A. Taube, M. Wzorek, *Micromachines* **9**, 546 (2018).
- [93] A. Taube, M. Kozubal, J. Kaczmarek, M. Juchniewicz, A. Barcz, J. Dyczewski, R. Jakiela, E. Dynowska, M. Borysiewicz, P. Prystawko, J. Jasiński, P. Borowicz, E. Kamińska, A. Piotrowska, *Mater. Res. Soc. Symp. Proc.* **1635**, 9 (2014).
- [94] A. Taube, E. Kaminska, M. Kozubal et al., *Phys. Status Solidi (a)* **212**, 1162 (2015).
- [95] D. Gryglewski, W. Wojtasiak, E. Kamińska, A. Piotrowska, *Electronics* **9**, 1305 (2020).